COLD FLOW DETERMINATION OF THE INTERNAL FLOW ENVIRONMENT AROUND THE SUBMERGED TVC NOZZLE FOR THE SPACE SHUTTLE SRM

R. H. Whitesides, A. Ghosh* and S. L. Jenkins
SRS Technologies
Huntsville, Alabama

and

D. L. Bacchus
NASA Marshall Space Flight Center
Huntsville, Alabama

ABSTRACT

A series of subscale cold flow tests was performed to quantify the gas flow characteristics at the aft end of the Space Shuttle Solid Rocket Motor. This information was used to support the analyses of the redesigned nozzle/case joint. A portion of the thermal loads at the joint are due to the circumferential velocities and pressure gradients caused primarily by the gimbaling of the submerged nose TVC nozzle. When the nozzle centerline is vectored with respect to the motor centerline, asymmetries are set up in the flow field under the submerged nozzle and immediately adjacent to the nozzle/case joint. Specific program objectives included: 1) Determine the effects of nozzle gimbal angle and propellant geometry on the circumferential flow field. 2) Measure the static pressure and gas velocities in the vicinity of the nozzle/case joint. 3) Use scaling laws to apply the subscale cold flow data to the full scale SRM, and 4) Generate data for use in validation of 3-D computational fluid dynamic, CFD, models of the SRM flow field.

These tests were conducted in the NASA Marshall Space Flight Center Airflow Facility with a 7.5 percent scale model of the aft segment of the SRM. Static and dynamic pressures were measured in the model to quantify the flow field. Oil flow data was also acquired to obtain qualitative visual descriptions of the flow field. Nozzle gimbal angles of 0°, 3.5°, and 7° were used with propellant grain configurations corresponding to motor burn times of 0, 9, 19 and 114 seconds.

This experimental program was successful in generating velocity and pressure gradient data for the flow field around the submerged nose nozzle of the Space Shuttle SRM at various burn times and gimbal angles. The nature of the flow field adjacent to the nozzle/case joint was determined with oil droplet streaks, and the velocity and pressure gradients were quantified with pitot probes and wall static pressure measurements. The data was applied to the full scale SRM thru a scaling analysis and the results compared well with the 3-D computational fluid dynamics computer model.

INTRODUCTION

A series of subscale tests was performed to quantify the gas flow characteristics in the SRM aft section. The information obtained as a result of these tests, and the analyses conducted thereafter, have been used to support the SRM joint redesign. The redesigned nozzle/case joint was subjected to flow and thermal analyses in order to verify the adequacy of the new design. The thermal loads on the joint consist of 1) the initial pressurization during the ignition transient and 2) the secondary flows in the joint during motor operation which could be caused by asymmetric circumferential pressure distribution. Of course, there would be no flow in the joints for a completely bonded joint; however, the analyses must consider possible defects or "blow-holes" in the joint interfaces between motor segments. The flow and heating along the "blow-hole" paths and around the O-ring groove depend on the circumferential pressure differential. The cause of the circumferential pressure and velocity gradients at the nozzle/case joint is the gimbaling of the TVC nozzle. When the nozzle centerline is vectored with respect to the motor centerline, asymmetries are set up in the flow field under the submerged nozzle and immediately adjacent to the nozzle/case joint. The measured circumferential pressure and velocity distributions were compared with CFD computations in order to validate the CFD predictions for the full scale SRM. Also, the test results were used with scaling laws to quantify circumferential pressure differentials for the full-scale SRM.

This series of tests was conducted in the NASA Marshall Space Flight Center SSME Airflow Facility. Nozzle gimbal angle and propellant configuration were variables in the test program which used a 7.5% model of the aft section of the solid rocket motor. Circumferential and axial total, static and dynamic pressures were measured in the model to quantify the flow in the model. Oil flow data was also acquired to obtain qualitative descriptions of the flow.

The data reduction process included statistical "filtration" of the test data using a "Ratio Test" method for small data

---

This work was performed under USBI Booster Production Company Contract No. H08515 (NAS8-36300) for the George C. Marshall Space Flight Center of the National Aeronautics and Space Administration. The support of Mr. Jack Hengel as Test Engineer and other NASA/Marshall Air Flow Facility testing and instrumentation personnel is gratefully acknowledged.
* A. Ghosh is currently employed by Rockwell International Corporation, Rocketdyne Division, Canoga Park, California.

sample sizes. An uncertainty analysis was conducted to obtain estimates of the uncertainty in the data presented. A scaling analysis was carried out to determine the applicability of cold flow subscale test results to the full scale motor, and to calculate the circumferential pressure gradients in the full scale motor.

More detailed descriptions of these tests and test results are presented in the Test Data Report [1], and the Final Data Analysis Report [2].

OBJECTIVES

The objective of this series of tests was to determine the internal flow characteristics (pressures and velocities) in the aft end of the SRM model. Specific objectives were as follows:

- Investigate the effects of nozzle gimbal angle and propellant geometry on circumferential flow in the aft motor section.
- Measure the static and total pressure variations in the vicinity of the nozzle/case joint for nozzle gimbal angles of 0°, 3.5°, and 7° and propellant configurations corresponding to motor burn times of 0, 9, 19, and 114 seconds.
- By appropriate data reduction and scaling quantify the circumferential pressure gradient at the aft end of the full scale RSRM.
- Generate data to validate the 3-D CFD models which will be used to predict the full scale RSRM flow fields and boundary conditions for the detailed nozzle/case joint insulation gap flow and thermal analyses.

COLD FLOW MODEL AND TEST FACILITY

MODEL CONFIGURATION

The cold flow test article was a 7.5% scale model of the aft section of the RSRM. The test section assembly consists of an outer case, propellant grain simulators, facility to test section port transition, nozzle assembly and nozzle cant angle rings. An assembly sketch of the model appears in Fig. 1. Shown in Fig. 1 are the propellant grain simulators representing the grain geometry at the four burn times indicated. The propellant burn times tested are 0, 9, 19, and 114 second configurations. The 114 second configuration (empty case) has a diameter of 0.2659 m (10.469 in.), and represents the diameter of the insulation surface. Nozzle gimbal angles tested are 0, 3.5, and 7 degrees. The nozzle throat diameter is 0.1026m (4.04 in.). The nozzle cant angle rings were used to hold the nozzle at 0°, 3.5° and 7° with respect to the model axis. A transition assembly was used as an interface between the 0.4064 m (16 in.) facility pipe to the lesser diameters of the propellant grain simulators in the model.

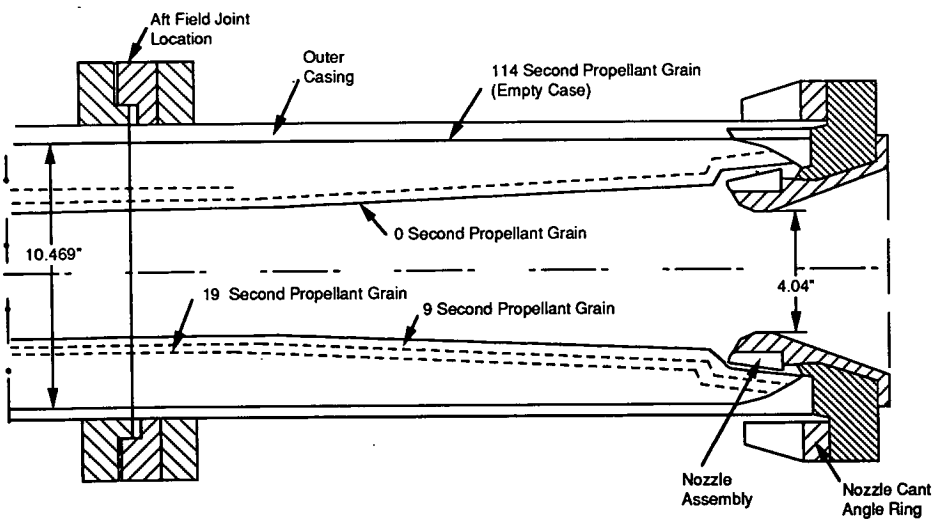

FIGURE 1. SPACE SHUTTLE SRM MODEL ASSEMBLY

TEST FACILITY

The test facility used for this series of tests was the Space Shuttle Main Engine Air Flow Facility located at the NASA Marshall Space Flight Center. Ambient temperature air is delivered to the test section through a 0.4064m (16 in.) diameter pipe connected to the main supply tank which can be pressurized to 2999 KPa (435 psia). Flow is regulated by an automatic pressure control valve in the main supply line. Since the supply tank is bled down as any particular run proceeds, the controlling valve has to be opened with time to maintain a constant pressure (e.g., 2413 KPa (350 psia)) downstream of the valve. Approximately 48.5 kg/sec (107 lbm/sec) of air at ambient temperature was delivered to the test article for approximately 18 seconds.

INSTRUMENTATION

The instrumentation used consists of temperature and pressure measurement devices. Thermocouples were used to make the air temperature measurements. Total pressures were measured with pitot probes and static pressures were measured at wall ports. Differential pressure transducers with operating ranges of 0-68.9 KPa (0-10 psi), 0-103.4 KPa (0-15 psi) and 0-310.3 KPa (0-45 psi), and absolute pressure transducers with an operating range of 0-3447 KPa (0-500 psia) were utilized for the pressure measurements. The reason for using differential pressure transducers was to be able to accurately measure the small pressure differentials expected between different regions of the flow.

TEST PROGRAM

CALIBRATION TESTS

The test model was calibrated prior to testing. The purpose of the calibration tests was to measure inlet total pressure profiles and to demonstrate symmetry in flow patterns with axisymmetric geometries. The tests were performed with each grain, using the zero degree nozzle. The total pressure was surveyed radially in the horizontal and vertical planes at one section upstream of the test section. The pressure traverses were made on two perpendicular radii on both sides of the center. Four points on each side of the centerline and one at the center were surveyed with pitot probes. Static pressures were taken from wall taps at these circumferential locations. The calibration tests were also intended to allow verification of model flow rate and mach number.

It was found that slight asymmetries in the flow existed even with purely axisymmetric geometries. Several attempts were made to correct this problem. It was concluded, after several trial runs, that the asymmetries were probably caused by two factors. These were:

(1) Flow disturbances caused by the control valve upstream of the model.
(2) The non-symmetric or skewed fit of the model in the facility pipe, i.e., the axis of the model was not precisely aligned with the axis of the facility.

However, the pressure differential caused by non-zero nozzle angles is significantly greater than any pressure differentials created by the factors mentioned above. Therefore, the asymmetries observed were not considered significant enough to preclude a reasonable data correction.

OIL FLOW TESTS

Subsequent to the calibration tests, oil flow tests were performed. These tests were conducted to determine the local flow direction at different sections in the model. The local flow directions obtained from the oil flow tests were used to align the total pressure probes at these sections for the fully-instrumented tests. Subsequent to initial checkout and calibration runs each test configuration was oil flow tested to determine the local flow direction. The oil streaks were photographed and videotaped for evaluation of flow direction and to maintain a permanent record of the flows. The angle of the flow at each instrumentation station was measured with a special tool and recorded. These angles were used later to align the total pressure probes at the measurement locations in the model.

FULLY-INSTRUMENTED NOZZLE TO CASE JOINT TESTS

These series of tests were designed to evaluate the pressure and velocity characteristics of the flow in the aft motor section, specifically in the region of the nozzle to case joint. Of particular interest is the circumferential flow in the region of the aft joint. The fully instrumented test series for the aft nozzle section consisted of all combinations of three nozzle gimbal angles, 0°, 3.5°, and 7°, and four motor burn time propellant geometries, 0 sec, 9 sec, 19 sec, and 114 sec, for a total of 12 combinations or test conditions. Two runs were generally made for the fully-instrumented nozzle to case joint tests. The purpose of this was twofold: first, to check repeatability of the data, and second, to provide for the possibility of combining the data from both runs in order to obtain a larger data sample size for statistical averaging of measured differential pressures which can be expected to lead to more accurate results.

Test reference conditions, calculated velocity, Mach number, etc., and relevant geometrical parameters at a section just upstream of the nozzle entrance, are given in Table I.

TABLE I. MODEL GEOMETRY, REFERENCE CONDITIONS, AND CALCULATED PARAMETERS

Propellant Grain	0 Second	9 Second	19 Second	114 Second
Parameter				
Throat Diameter, m (in.)	0.103 (4.04)	0.103 (4.04)	0.103 (4.04)	0.103 (4.04)
Section Diameter, m (in.)	0.161 (6.33)	0.174 (6.84)	0.1886 (7.426)	0.2659 (10.469)
Area Ratio	2.455	2.866	3.379	6.715
γ	1.4	1.4	1.4	1.4
Reference Pressure, KPa (psia)	2413 (350)	2413 (350)	2413 (350)	2413 (350)
Reference Temperature, °K (°R)	278 (500)	278 (500)	278 (500)	278 (500)
Calculated Mach Number	0.24427	0.20713	0.17443	0.08657
Calculated Static Pressure KPa (psia)	2315.1 (335.77)	2342.1 (339.69)	2362.5 (342.65)	2400.6 (348.17)
Calculated Average Velocity, m/sec (ft/sec)	81.600 (267.73)	69.192 (227.02)	58.268 (191.18)	28.92 (94.88)
Calculated Mass Flow Rate, kg/sec (lbm/sec)	48.39 (106.7)	48.39 (106.7)	48.39 (106.7)	48.39 (106.7)

DATA RECORDING AND REDUCTION

DATA RECORDING

The pressure measurement system used was a multiple-channel scanning system manufactured by PSI, Inc. This system is capable of scanning 292 channels of pressure data in 100 milliseconds. In the present test, 103 channels were used. The data acquisition/control system was a Hewlett Packard 3054A system.

The data acquisition system took ten frames of data for every run. In each of these ten frames, 20 scans of all channels being used were made by the PSI system. The time taken for 1 scan was about 100 milliseconds. Thus, for the 103 channels used in this test, the system would scan in sequence channels 1 through 103 once, store the pressure data, pause to reset, the start the next scan over channels 1 thru 103. This data would then also be stored, and the whole process repeated 20 times. When 20 scans had been completed, data for 1 frame would have been obtained. The system would start all over again for the second frame, and repeat the process outlined for Frame 1. The process would go on until all 10 frames of data had been obtained and stored. This generally took around 18 seconds. During the on-line data reduction process, the data acquisition/control system took the 20 values of each measurement (channel) for each frame, and computed an arithmetic average, and stored it. It did the same for all 103 channels. Thus, at the end of the on-line data reduction process, there were ten frames of data, for each of 103 channels. The digital test data was then reduced and stored in engineering units such as psi, psia, °R, seconds, etc., and transferred to a 9-track, 1600 BPI, ASCII format magnetic tape at the test facility.

DATA REDUCTION

Nineteen pressures (static and total) were measured on 0-3447 KPa (0-500 psia) transducers. All other static and total pressures were measured as pressure differentials between selected reference pressures and the pressure to be measured. The required pressure was then obtained by adding (or subtracting) the measured differential pressure to (or from) the reference pressure, since a differential pressure can be positive or negative.

The measured quantities in the nozzle/case joint tests are temperatures (T), static pressure (p_s), total pressures (p_t), and differential pressures (Δp). From these measurements, static, dynamic and total pressures, Mach number, static temperature, velocity magnitude, and pressure coefficient were calculated at different points in the model. The equations used to calculate the Mach number, dynamic pressure, static temperature, velocity and pressure coefficient were derived from the basic compressible, inentropic equations. A data reduction program was developed by SRS Technologies to reduce the data from the fully-instrumented tests. The program consisted of routines which read in the raw data, normalized and referenced to 2413 KPa (350 psia) the static, total and differential pressures, corrected the total temperature upstream of the model (and downstream of the valve), statistically filtered and averaged the measured pressures, calculated local static, dynamic and total pressures, circumferential Δp's, Mach numbers, temperatures, velocity magnitudes and pressure coefficients.

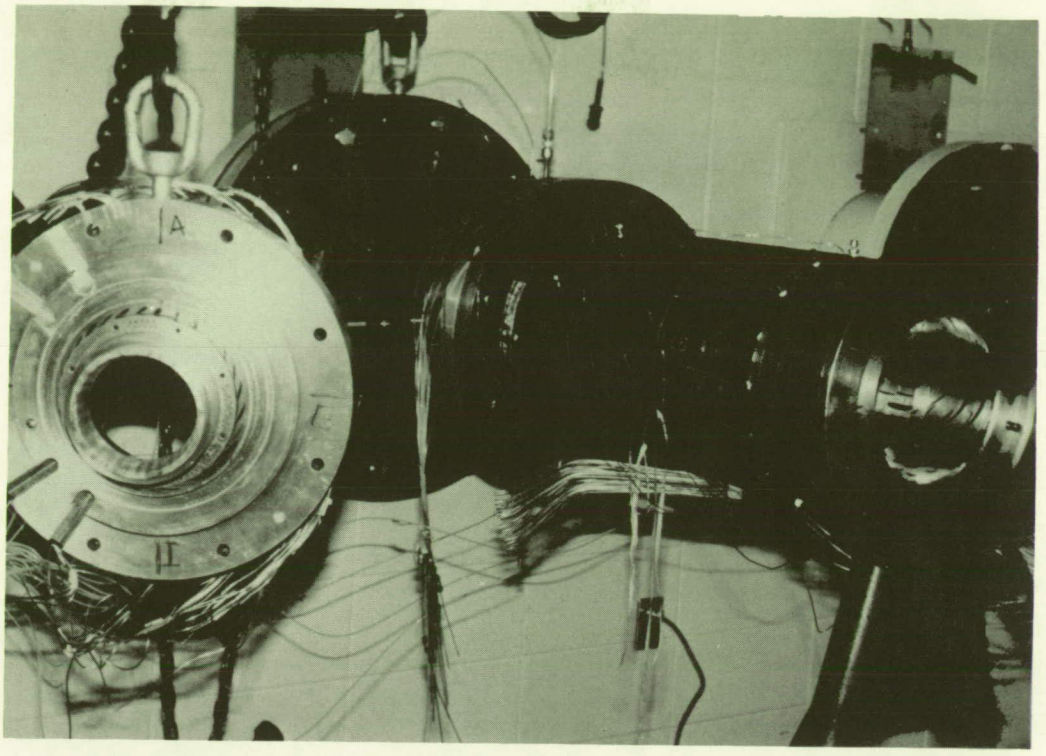

Fig 2. SRM Cold Flow Test Model

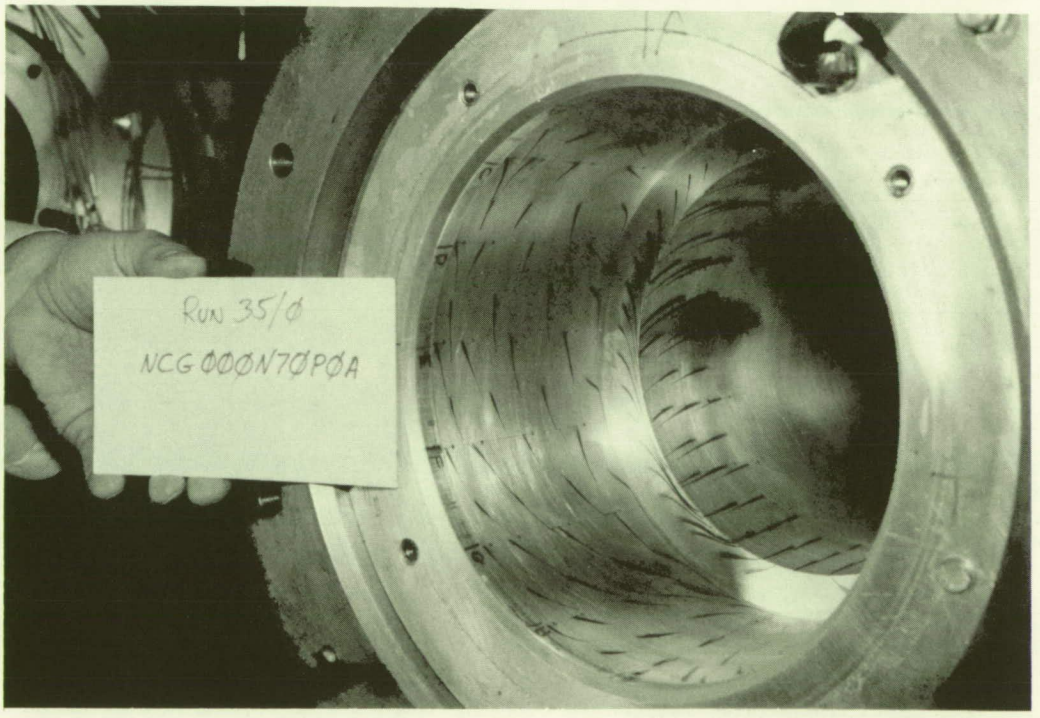

Fig 3. Oil Flow Pattern in Lower Half of Propellant Grain, Aft End; Propellant Grain = 0 Sec, Nozzle Angle = 7°

Fig 4. Oil Flow Pattern on Nozzle Nose; Propellant Grain = 0 Sec, Nozzle Angle = 7°

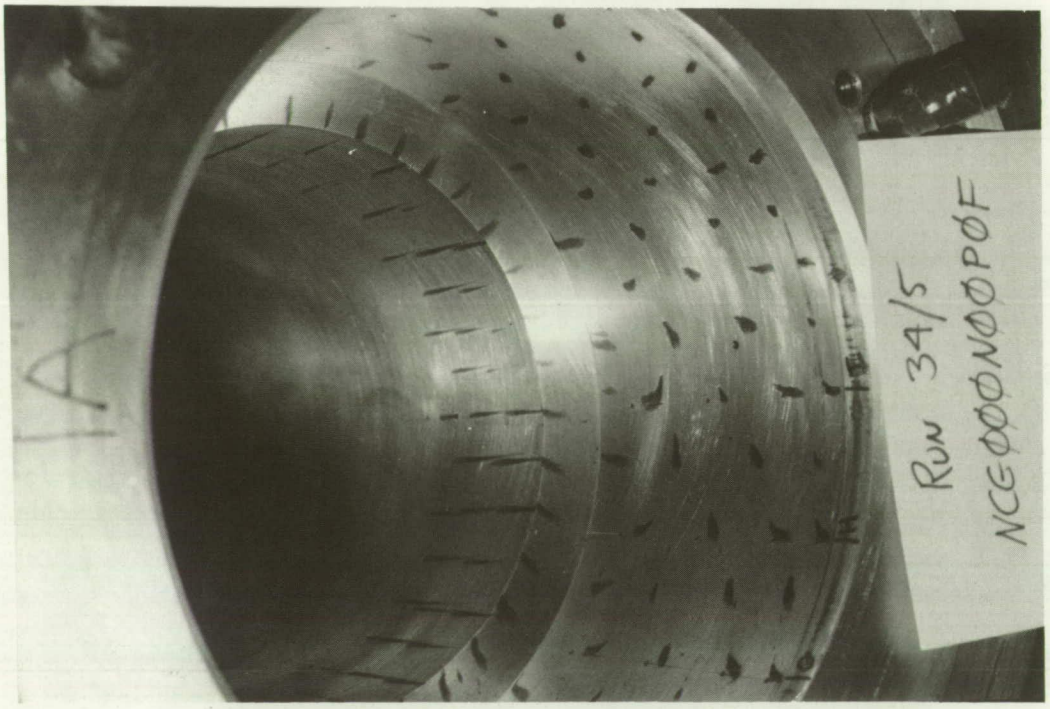

Fig 5. Oil Flow Pattern in Lower Half of Propellant Grain, Aft End; Propellant Grain = 0 Sec, Nozzle Angle = 0°

Fig 6. Oil Flow Pattern in Lower Half of Propellant Grain, Aft End; Propellant Grain = 0 Sec, Nozzle Angle = 3.5°

Fig 7. Oil Flow Pattern in Lower Half of Propellant Grain, Aft End; Propellant Grain = 0 Sec, Nozzle Angle = 7°

For each of the 10 frames of measured data, a total pressure (and wall static pressure) were measured by probes placed at the 0°, 90° 180°, and 270° angular positions. An arithmetic average of these four total pressures was then computed for each frame. Thus, for ten frames there were ten such average pressures, one corresponding to each frame. These ten averages were then plotted against the frame number. Since these ten points on the plot did not fall on a smooth curve, a polynomial curve fitting routine was then used to draw a smooth curve as a best approximation to the ten computed average pressures. This then yielded a correct average total pressure for each frame. The measured static and total differential pressures in the model were subsequently normalized by this corrected average pressure (for each frame), and referenced to 2413 KPa (350 psia).

A reference temperature of 278 °K (500°R) was used to compute the velocity magnitude. Since the temperature varied from run to run, it was thought worthwhile to reference the velocity computation to a constant temperature to make comparisons easier. The value 278 °K (500°R) was arrived at by averaging the first and tenth frame temperature data for all fully-instrumented runs in the nozzle/case joint tests.

A review of the raw data gathered from some nozzle/case joint tests revealed the occurrence of outliers - extreme observations in the data samples over the specified number of frames. Since the use of invalid data points can provide erroneous results, a statistical method to determine and reject the outliers was seen as a necessary function in the data reduction procedure. There are several widely-used methods available to handle this problem in cases where the sample size (number of frames in this case) is large, but few methods exist to handle this problem in cases with small sample sizes. A literature review yielded the few available methods and their algorithms. These methods were scrutinized as to their applicability to the current effort and the ratio test emerged as the most appropriate method:

The ratio test is a statistical algorithm which compares "the distance of one end observation from its neighbors with the range of all, or all but one or two, of the observations" [3]. The ratio test was chosen because it checks both the upper and lower bounds of the data sample (over the number of frames) before manipulating the data to remove outliers. This is more desirable because it ensures that all valid data will be used.

TEST RESULTS

OIL FLOW RESULTS

Every configuration was oil flow tested before total pressure probes were installed. These tests served a dual purpose. First, they provided visual qualitative data on the flowfields which was recorded on both photographs and videotape. Second, they served to quantify the angle of the local velocity vector at any point in the model. Following each oil flow run, the flow patterns were photographed and videotaped; thereafter, the angles indicated by the oil streaks were measured by a specially devised protractor, and recorded. For the fully-instrumented pressure survey tests, the total pressure probes were aligned in accordance with the angles measured and recorded from the oil flow tests.

For non-zero nozzle gimbal angles, the nozzle was vectored such that the nozzle nose moved downward which created a wider gap between the nozzle nose and the propellant grain at the top (0°) of the model. For all configurations that had non-zero nozzle gimbal angles, the flows had a vertical plane of symmetry. The 0° position is angular station A, the 90° position is angular station E, the 180° position is angular station I, and the 270° position is angular station J. Other letters indicate positions between 0° and 90°, between 90° and 180°. Letters indicating angular positions can be seen on the oil flow photographs. In the oil streaks on all oil flow photographs, the upstream part of the local flow is indicated by the wide part, or head, of the streak, and the downstream part by the thin part, or tail, of the streak.

Fig. 2 shows the model with the nozzle section removed. Oil flow patterns are visible on the nozzle inlet and on the propellant grain simulator underneath the submerged nose nozzle. When the nozzle is gimballed to 3.5 degrees or 7.0 degrees, the nose of the nozzle tilts downward which leaves a larger gap between the nozzle nose and the propellant grain simulator at the top or the zero degree (A) position. The flow enters this gap at the top then turns circumferentially around the sides and finally reverses and flows forward near the bottom of the 180 degree position. The resulting flow patterns on the propellant grain simulator is shown in Fig. 3 for a gimbal angle of 7.0 degrees. The corresponding flow pattern on the outer nozzle nose surface is shown in Fig. 4. Figures 5, 6, and 7 are views of the lower half of the propellant grain simulator looking into the aft end for a burn time of zero seconds. The nozzle gimball angles for these three figures are 0, 3.5, and 7.0 degrees, respectively. The bulk flow is toward the viewer. The flow on the grain surface upstream of the nozzle nose and the step in the grain contour is parallel to the model axis. However, the flow in the cavity between the nozzle nose and the propellant grain is circumferential in the lateral zones, as the flow moves from the top, 0°, toward the bottom, 180°, where it reverses and flows back forward. The magnitude of the circumferential flow velocities, as indicated by the length of the oil flow streaks, increases with nozzle gimbal angle. Some circumferential flow is shown in Fig. 5 even for a zero degree gimbal angle due to asymmetries in the model flow field.

RESULTS FOR MEASURED FLOW PARAMETERS

In Figs. 8, 9, and 10, the circumferential static pressure distribution, the difference in static wall pressure between any given location and the zero degree location, is plotted versus the angular location in degrees. The axial station is at the extreme aft end of the cavity between the nozzle and the propellant adjacent to the case/nozzle joint. The nozzle gimbal angle for these

for bias corrections made to the data for gimbal angles of 3.5 and 7.0 degrees. Maximum velocities and minimum pressure generally occurred between 110 and 135 degrees. A stagation zone occurs near 180 degrees where the flow reverses and goes forward. Velocities drop and pressure rises as the flow approaches the 180 degrees position. These figures show that the zero second burn time propellant grain configuration does not necessarily produce the highest circumferential flow activity even though the axial port velocity and dynamic pressure is highest at this condition. This is due to the fact that the propellant grain shields the nose of the nozzle at the zero second burn time. In other words, the nose of the nozzle does not protrude up into the flow at zero burn time. Also the gap width of the cavity between the nozzle and the propellant is dimimished at zero seconds. The effect of cant angle on the circumferential pressure and velocity gradients is shown directly in Figs.14 and 15 for a burn time of 9 seconds.

Figures 16 and 17 present summary plots for the 3.5° and 7° nozzle TVC angles. Each of these figures shows the variation of the circumferential pressure difference ($P_{s\theta}$° - P_{s0}°) as a function of propellant burn time. For a nozzle gimbal angle of 3.5°, Fig. 16 shows that the circumferential Δp, defined as ($P_{s\theta}$° - P_{s0}°), reaches a maximum at a burn time of 19 seconds. The maximum Δp at 19 seconds burn time occurs at the 157.5° and 180° angular locations, and the magnitude of this Δp_{max} is about 5.79 KPa (0.84 psi). A similar study of Fig. 17 shows that here the circumferential Δp reaches a maximum value at the 135° angular location and is almost constant between burn times of 9 to 19 seconds. The maximum Δp at the 135° angular location is about 10.1 KPa (1.46 psi).

Previous figures showed that even for a 0° nozzle TVC angle, there is a non-zero circumferential Δp. This leads to the possibility that the flows for nozzle TVC angles of 3.5° and 7° were also "biased" by this asymmetry in the flow that exists for a 0° nozzle TVC angle. A corrections was performed for the data in Figs. 16 and 17 by simply subtracting the Δp for the 0° nozzle gimbal angle flow from the Δp's for the 3.5° and 7° nozzle TVC angle flows. The effect of the bias correction was to reduce the magnitudes of the circumferential Δp's.

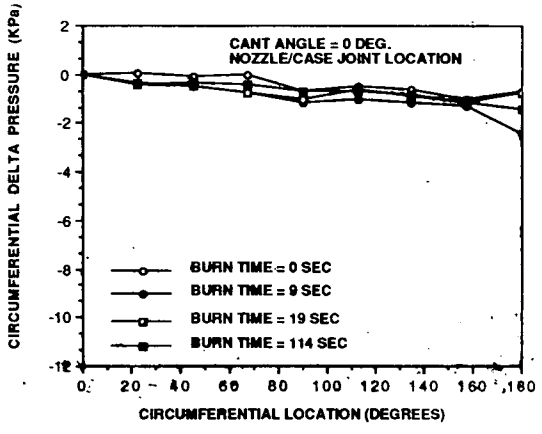

Fig 8. Circumferential Pressure Distribution ($P_{s\theta}$ - P_{s0}°)

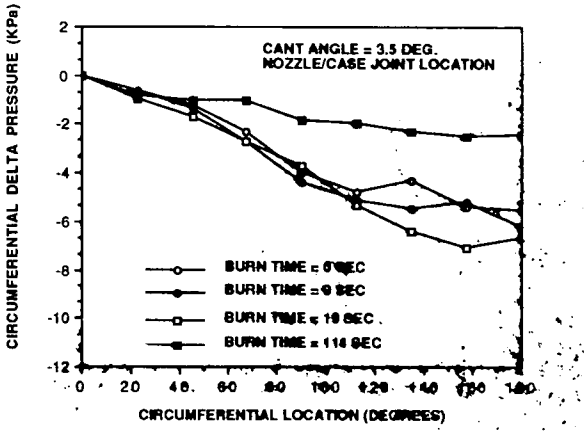

Fig 9. Circumferential Pressure Distribution ($P_{s\theta}$ - P_{s0}°)

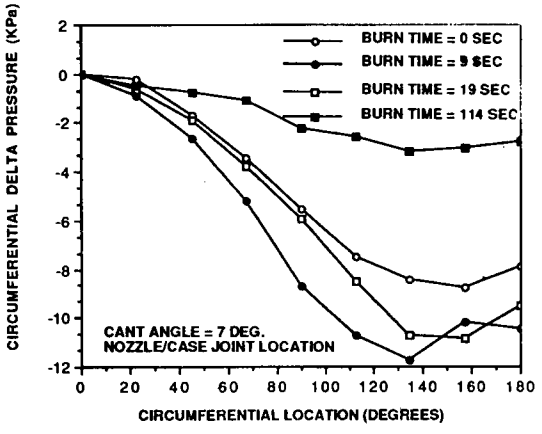

Fig 10. Circumferential Pressure Distribution ($P_{s\theta}$ - P_{s0}°)

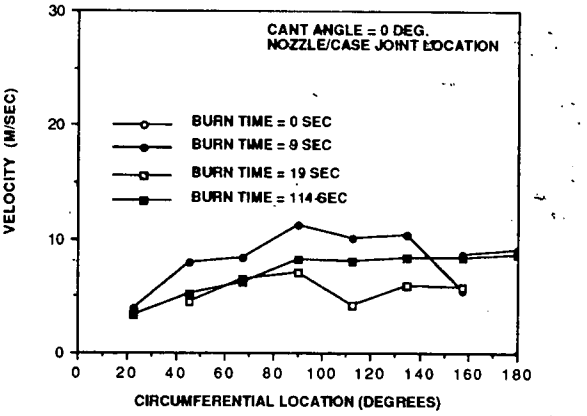

Fig 11. Circumferential Velocity Distribution

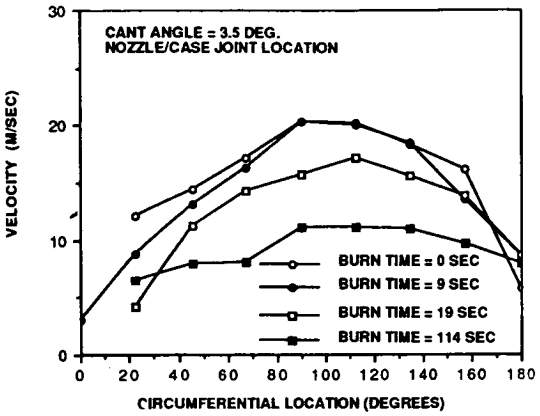

Fig 12. Circumferential Velocity Distribution

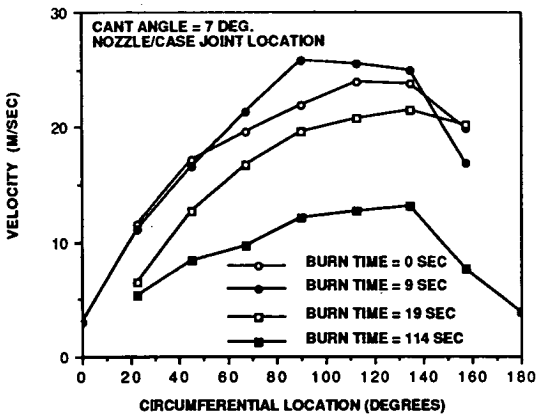

Fig 13. Circumferential Velocity Distribution

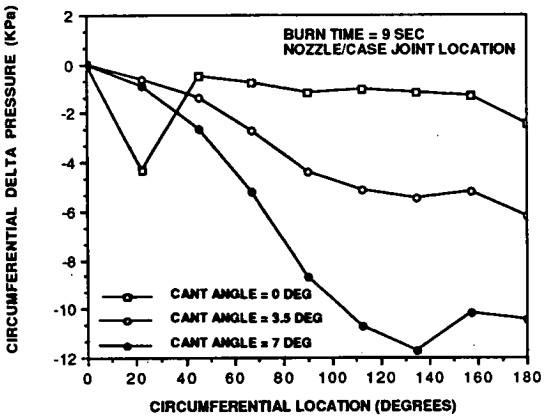

Fig 14. Circumferential Pressure Distribution ($P_{s\theta}$ - $P_{s0°}$)

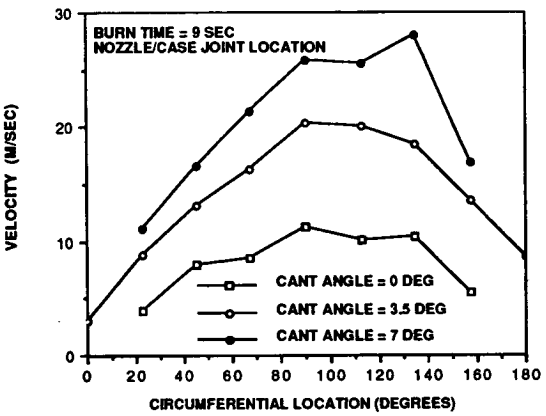

Fig 15. Circumferential Velocity Distribution

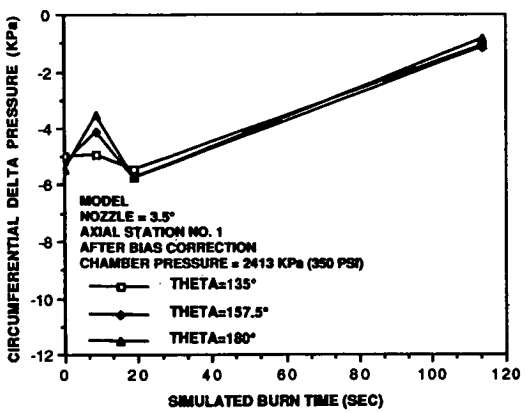

Fig. 16 Circumferential ΔP ($P_{s\theta}$ - $P_{so°}$) VS. Burn Time

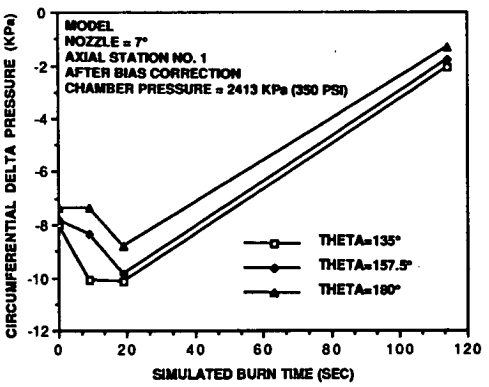

Fig. 17 Circumferential ΔP ($P_{s\theta}$ - $P_{so°}$) VS. Burn Time

SCALING ANALYSIS

It is of interest to know how measurements made in the subscale model and cold flow tests can be applied to the full-scale solid rocket motor where the fluid medium is different from that used in the cold flow tests. Ambient temperature air was the test fluid in the latter. Parameters of interest are the static and dynamic pressure distributions in the SRM aft section. For the present analysis viscous effects will be neglected in scaling the nozzle to case joint data.

Characteristics of the SRM are as follows:

TIME (sec)	M	q KPa (Psi)	P KPa (Psia)
0	0.2512	199.2 (28.89)	5543 (804)
9	0.2132	145.2 (21.06)	5619 (815)
19	0.1796	104.4 (15.14)	5688 (825)
114	0.0892	8.48 (1.23)	1868 (271)

The cold flow model conditions at similar area ratios are as follows:

TIME (sec)	M	q KPa (Psi)	P KPa (Psia)
0	0.2443	96.67 (14.02)	2137 (336)
9	0.2071	70.3 (10.20)	2344 (340)
19	0.1744	50.3 (7.30)	2365 (343)
114	0.0866	12.6 (1.83)	2399 (348)

The Mach numbers shown are just upstream of the nozzle entrance. Assuming equivalence in local pressure coefficients between the model and the motor due to geometric scaling and turbulent Reynolds numbers, the circumferential pressure differentials for the full scale motor were calculated from the measured model pressure by the dynamic pressure scaling equation:

$$\Delta P_M = \Delta P_m * (\gamma_M / \gamma_m) * (P_{refM} / P_{refm}) * (M_{refM} / M_{refm})^2$$

where the subscript "M" is for the motor and "m" is for the model

COMPARISON OF SCALED COLD FLOW DATA WITH COMPUTATIONS OF THE FULL-SCALE SRM

A comparison of the full scale RSRM circumferential pressure differentials as determined from the cold flow data scaling analysis and as determined from various computational fluid dynamic, CFD, analyses is presented in Fig. 18. These CFD analysis results were obtained by four organizations using three different computer codes. Continuum's CONTINUSYS code results were taken from Reference 4. The results from Creare's FLUENT code are presented in Reference 5. Both the CFD Research and Morton Thiokol results were obtained with different versions of the PHOENICS code and are presented in Reference 6 and 7, respectively. The scaling analysis results compare with some CFD results better than others. Variations between the given motor port pressure and velocity for the various analyses is responsible for a portion of the difference. The most favorable comparison is for the 3.5 degree gimbal angle which is of more direct interest. The best comparison with CFD results include the Creare results and the MTI results. The CFD results are generally lower which is probably due primarily to the effects of mass addition which are not included in the scaling analysis. There is more scatter in the comparisons at the 7 degree gimbal angle. The comparisons between all results are more favorable, generally, at the higher burn times when the circumferential pressure differential is less. Also at the higher burn times, the effect of mass addition due to propellant burning underneath the submerged nozzle is less since the confined space between the nozzle and the propellant grain opens up considerably as burn time increases.

CONCLUSIONS

The following general conclusions have been drawn from this test series:

(1) For a nozzle gimbal angle of 3.5°, the maximum circumferential Δp, defined as $P_{S\theta} - P_{S0°}$, occurs at a burn time of 19 seconds, at an angular location of 157.5°. The value of the Δp (maximum) scaled to the RSRM is -12.00 KPa (-1.74 psi).

(2) For a nozzle gimbal angle of 7°, the maximum circumferential Δp, defined as $P_{S\theta} - P_{S0°}$, occurs at a burn time of 9 seconds, at an angular location of 135°. The value of this Δp (maximum) scaled to the RSRM is -20.96 KPa (-3.04 psi).

(3) For burn times greater than 19 seconds, the circumferential Δp, defined as above, decreases significantly to a minimum value at burnout less than 0.90 KPa (0.13 psi) for a gimbal angle of 3.5 degrees.

(4) Slight asymmetries were seen in the flow with a nozzle gimbal angle of 0°. The data for other values of the nozzle gimbal angle have been corrected by subtracting out this bias that was experienced for the 0° gimbal angle.

(5) The asymmetry mentioned above was probably created by a slight skewness of the model relative to the facility pipe, and/or by flow nonuniformity from a control valve upstream of the model.

(6) The circumferential Δp's for the full-scale RSRM are obtainable from the corresponding circumferential Δp's for the subscale model through a simple algebraic expression derived from the scaling analysis. Acceptable comparisons between the scaling analysis and the CFD analyses for the full scale RSRM were obtained.

(7) Oil flow tests were very useful because they provided qualitative descriptions of the flows, provided a permanent record of the flows, and provided local flow directions in the propellant grain.

(8) The overall experimental program including the testing, the oil flow visualization, the data reduction and the data analysis, was successful in obtaining a significant amount of data and information which was scaled up and applied to the full scale RSRM.

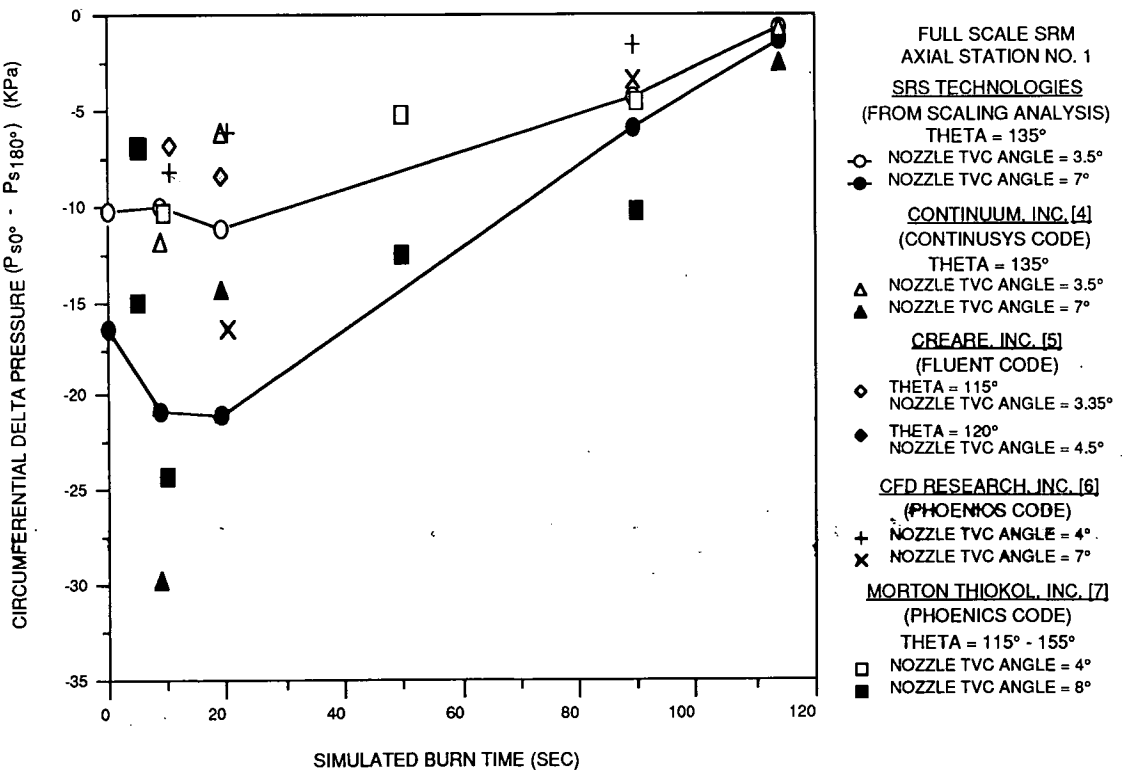

Fig 18. Comparison of Scaling Analysis Results with CFD Results for the Full Scale SRM

REFERENCES

1. Test Data Report, Subscale Cold Flow Tests, 3-D Aft Motor Cases (SRM D MSFC 21, Phase I), SRS Technologies Report, SRS/STD-TR87-78, NASA/Marshall Space Flight Center-RPT-1509, July 1987.

2. Final Data Analysis Report, Subscale Cold Flow Tests, Aft Field Joint (MSFC Test 21, Phase II), SRS Technologies Report, SRS/STD-TR88-13, NASA/Marshall Space Flight Center-RPT-1512, November 1987.

3. Wilfred J. Dixon, and Frank J. Massey, Jr., Introduction to Statistical Analysis, 3rd Ed. (New York: McGraw-Hill Book Co., 1969).

4. Three-Dimensional SRM Case/Nozzle Joint Flow Field Analysis (NASA/MSFC Contract No. 7MG041) Continuum, Inc. Final Report, CI-FR0D101-02, July 1987.

5. "Prediction of the Circumferential Pressure Gradient in the Vectored Nozzle Flowfield", Creare, Inc., Presented at the Space Shuttle SRM Circumferential Flow Technical Interchange Meeting, Morton Thiokol MTC, Odgen, Utah, September 29-30, 1987.

6. "A CFD Analysis of the Space Shuttle SRM Aft-End Region", CFD Research Corporation presented at the Space Shuttle SRM Circumferential Flow Technical Interchange Meeting, Morton Thiokol MTC, Odgen, Utah, September 29-30, 1987.

7. "Circumferential Flow Near SRM Nozzle/Case Joint Due to Nozzle Vectoring", Morton Thiokol, Inc., presented at the Space Shuttle SRM Circumferential Flow Technical Interchange Meeting, Morton Thiokol MTC, Ogden, Utah, September 29-30, 1987.